Mon. Not. R. Astron. Soc. **268,** 345–353 (1994)

ROSAT observations of distant, optically selected galaxy clusters

Richard G. Bower,[1]★ Hans Böhringer,[1] Ulrich G. Briel,[1] Richard S. Ellis,[2] Francisco J. Castander[2] and Warrick J. Couch[3]

[1]*Max-Planck-Institut für Extraterrestrische Physik, Giessenbachstrasse, Garching bei München, Germany*
[2]*Department of Physics, University of Durham, South Road, Durham DH1 3LE*
[3]*School of Physics, University of New South Wales, Sydney, Australia*

Accepted 1993 December 10. Received 1993 December 2; in original form 1993 September 8

ABSTRACT

Evolution of the X-ray cluster luminosity function is investigated through X-ray observations of the Couch et al. catalogue of distant, optically selected galaxy clusters. A subset of 14 clusters provides a statistically complete sample, with mean redshift $\bar{z} = 0.42$, and a typical Abell richness of class 1–2. Observations of 12 of these clusters were secured using the *ROSAT* satellite in pointed mode; the remaining two clusters are analysed using data from the All Sky Survey. The X-ray emission from these clusters is surprisingly weak. The cluster luminosities are less than 5×10^{43} erg s^{-1} in all but two cases.†

We use a maximum-likelihood method to perform a quantitative comparison between our distant cluster luminosities and the present-day X-ray luminosity function derived by Henry et al. from the *Einstein* Extended Medium Sensitivity Survey. In the simplest case, where there is a direct relationship between optical richness and X-ray luminosity, our results imply a rise in the amplitude of the luminosity function by almost an order of magnitude since $z \simeq 0.4$. Even allowing for a significant scatter in the richness–L_X correlation, as observed locally, the distant data are inconsistent with the present-day luminosity function at the 3σ level. Our *ROSAT* data thus confirm the negative evolution of the luminosity function seen in the *Einstein* EMSS survey, and suggest that the steep slope in the high-redshift function may flatten off at luminosities below 10^{44} erg s^{-1}.

Key words: galaxies: clustering – galaxies: luminosity function, mass function – X-rays: galaxies.

1 INTRODUCTION

To understand the evolution of the X-ray properties of clusters of galaxies is one of the foremost goals of modern cosmology. A definitive measurement would provide fundamental constraints on models accounting for the origin of gravitational structure and the formation of galaxies. There are two aspects of particular interest: the cluster gas temperature function and the X-ray luminosity function (XLF). Although the evolution of the temperature function is more directly comparable with the predictions of *N*-body simulations (Frenk et al. 1990), only the XLF can be reliably measured with the current generation of survey telescopes.

As Kaiser (1986) describes, the evolution of the XLF is determined by the competition between two processes: the hierarchical growth of cluster masses, and the evolution of their internal characteristic density. Although standard cold dark matter (CDM) models (e.g. Davis et al. 1985) predict a marked decrease in the individual masses of rich clusters with redshift, the same clusters will have been more compact. Kaiser calculated that, since the total mass in 'clusters' must be conserved, the net effect is likely to be a rising XLF amplitude with redshift.

Despite its simplicity, this model does not reflect even the sense of the evolution observed in the X-ray cluster samples discussed by Edge et al. (1990) ($\langle z \rangle_{ev} \approx 0.13$) and Gioia et al. (1990) ($\langle z \rangle_{ev} \approx 0.33$). These studies found *fewer* X-ray luminous clusters at moderate redshifts than are found

★Present address: Royal Observatory, Blackford Hill, Edinburgh EH9 3HJ.
†We adopt $H_0 = 50$ km s^{-1} Mpc^{-1} and $q_0 = 0.5$ throughout.

locally. Henry et al. (1992, hereafter H92) argue that this evolution can still be accommodated within the self-similar model if it is assumed that the power spectrum of the initial linear density fluctuations was very flat. Alternatively, Kaiser (1991) has proposed that the evolution could be understood if the diffuse intracluster gas were reheated to 10^7 K at a redshift of ~ 5, and had only recently cooled sufficiently to become bound into the gravitational potential of a typical galaxy cluster. Models of this type, which break the scaling between the gas and gravitational mass, predict strong negative evolution of the luminosity function over a wide range of luminosities. The form of the evolution of the XLF at redshifts above 0.4 and luminosities below 10^{44} erg s^{-1} is thus an important point for observational attack.

One of the most important goals for the *ROSAT* satellite (Trümper 1985) is the independent confirmation of the earlier results published by Gioia et al. and Edge et al., as well as their extension to a greater redshift baseline and a larger range of cluster richnesses. In this paper, we present the first step: constraints on the evolution of the XLF to $\langle z \rangle \approx 0.4$ using Couch et al.'s (1991, hereafter CEMM) well-defined sample of *optically selected* rich clusters. Whilst X-ray-limited samples are clearly preferable in such studies, our procedure has the distinct advantage of economy. By defining in advance the position at which the X-ray flux is to be measured, it is not necessary to follow up each X-ray source in the survey area until a firm optical counterpart is identified. Elementary considerations show that, at the flux level required to detect distant clusters, they are outnumbered by AGN by a factor of *at least* 4:1 (cf. Stocke et al. 1991). Furthermore, we do not need to make firm detections of target clusters in order to constrain the evolution of the XLF: upper limits that lie below the expectation of a test luminosity function are still extremely important. The flux limit of the X-ray survey is thus set, not by the count rate at which sources may be reliably detected with low contamination rate, but by the background count rate in a *predetermined* area of the image. The X-ray follow-up of an optical sample has, of course, one serious drawback, namely that we must assume that the optical richness is sufficiently well correlated with the X-ray luminosity. We use the strength of the correlation observed at low redshift to quantify the extent of this uncertainty.

The paper is structured as follows. In Section 2, we describe our source of distant, optically selected rich clusters – the CEMM catalogue – emphasizing the large area of sky surveyed in its construction. In this section, we also discuss and review the philosophy of determining the XLF from a sample of *optically* selected clusters. Section 3 develops a maximum-likelihood method estimator for the XLF, which works directly from the observed photon counts. For a luminosity function of pre-defined shape, this method allows us to derive upper limits to the *amplitude* of the XLF. In Section 4, we discuss the *ROSAT* data on which this paper is based, and the methods used to determine the photon count-rate. We show that, if the strength of the correlation between X-ray and optical properties of these clusters is similar to that observed locally, our data are incompatible with the present-day XLF. In Section 5, we discuss the implications of this result, comparing our findings with the earlier results based on the *Einstein* Extended Medium Sensitivity Survey (EMSS). A summary of our conclusions is given in Section 6.

2 THE DISTANT CLUSTER SAMPLE

The CEMM catalogue of distant, optically selected clusters is the largest homogeneous sample of rich galaxy clusters in the redshift range $0.2 < z < 0.6$. Although the initial selection of candidate clusters was made by visual examination of deep IIIa-J and IIIa-F contrast-enhanced 4-m prime-focus plates, the final catalogue includes only clusters that pass a strict overdensity criterion (CEMM's 'σ' parameter). Extensive simulations and long-slit spectroscopy have verified the validity of this approach. While the Gunn, Hoessel & Oke (1986) catalogue presents a larger total sample of candidate clusters, including some of the most distant examples, their plate material was heterogeneous and their clusters were not identified with such well-defined procedures.

The total area surveyed by CEMM was 46 deg^2 (allowing for the overlap between their AAT J and F plates). They found 38 candidate clusters satisfying their overdensity criterion, $\sigma > 4$. Although redshifts have not yet been secured for all of these candidates, a strategy of obtaining complete redshift information within individual survey fields was adopted. Thus we may regard those clusters with redshifts and available X-ray data as a random subset of the full sample. 21 of the clusters with $\sigma \geq 4$ have accurate positions and reliable redshifts based on the spectra of more than one galaxy. We rejected the clusters J1836.23T and J1834.3TC, as the redshift measurements suggest that they are seriously affected by projection effects. We have assumed that, if the projection effects are taken into account, the individual components would not satisfy the enhancement (σ) criterion of the spectroscopic catalogue.

In order to calculate cluster space densities, it is important to account for the plates on which no clusters were found. For the incomplete redshift catalogue, we estimate this area via the fraction of the total area searched. For the 21 clusters for which positions and reliable redshifts are available, the effective survey area is 27.8 deg^2. These clusters cover a redshift range from 0.15 to 0.66, with a mean of $\bar{z} = 0.42$. In Fig. 1, the cumulative redshift distribution is compared with that expected for a volume-limited sample. As the figure shows, the sample suffers from incompleteness at redshifts above $z = 0.55$ and below $z = 0.25$, but the subsample in the range $0.3 < z < 0.5$ is well described by an approximately constant, comoving number density. By restricting our attention to this redshift interval, the X-ray properties of the subsample can be modelled by a single, spatially invariant XLF.

Our method is based on the assumption that the catalogued clusters are the richest systems in the volume surveyed, and are thus drawn from the high-luminosity tail of the XLF. Fig. 2 illustrates the projection of the bivariate L_X–optical richness distribution on to the XLF. In the highly idealized case, where the optical richness (or, strictly, the detectability parameter σ) correlates closely with the X-ray luminosity, L_X, the CEMM clusters will sample a well-defined wedge of the XLF. A more realistic approach is to model the scatter in the L_X–optical richness correlation by convolving the XLF with a Gaussian of fixed width (in log luminosity). The principal effect of this scatter will be to smooth out the cut-off of the effective XLF, as shown in Fig. 2.

In order to study the effects in detail, we use the L_X–optical richness correlations presented by Edge & Stewart (1991a,b). These authors found the galaxy richness, within a 3-Mpc metric radius (Abell 1958; Abell, Corwin & Olowin 1989), to be relatively poorly correlated with L_X. [This result is confirmed by the more recent work of Briel & Henry (1993): for the clusters that they reliably detected, we measure a scatter of a factor 2.5 in L_X at a given richness, but note that the dynamic range of these data is limited.] It is likely that this scatter is only partly intrinsic; see, for example, the discussion of Abell's richness classification in Lumsden et al. (1992). Edge & Stewart showed that the relationship becomes much tighter when the galaxy count is confined to a smaller region, such as the 0.75-Mpc radius sampled by CEMM in estimating their contrast factor (see Cappi et al. 1989). The scatter in L_X at fixed Bahcall number count (0.5-Mpc radius, Bahcall 1977) is a factor of 1.9 (rms, 0.5–2.5 keV band). As there will doubtless be significant

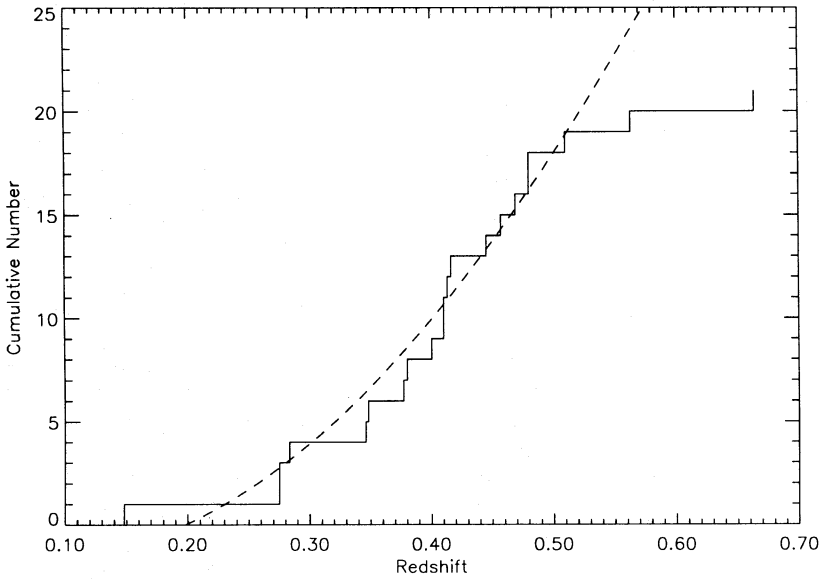

Figure 1. The cumulative redshift distribution for the sample of Couch et al. (1991) distant clusters studied in this paper. The dashed curve indicates the growth expected for a sample of constant, comoving number density.

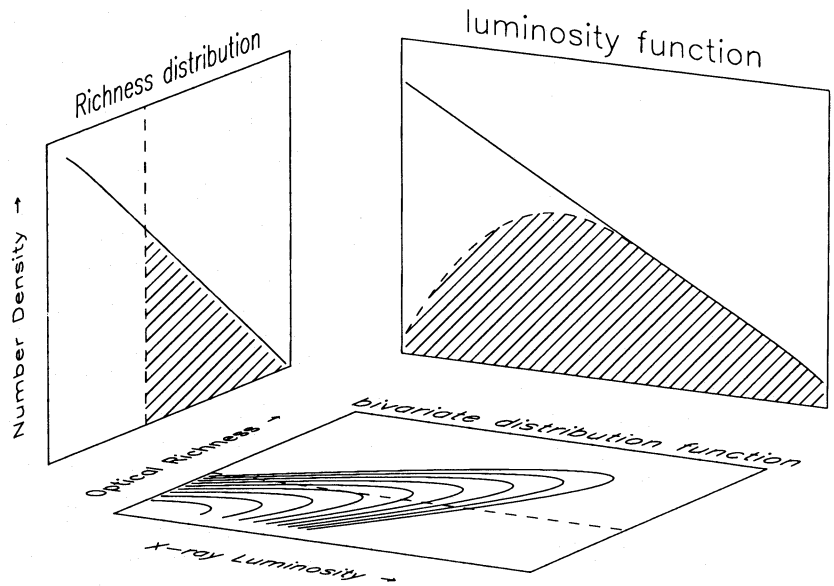

Figure 2. Illustration of the effect of using an optically selected sample to study the XLF of galaxy clusters. The horizontal plane shows a contour plot of the bivariate cluster optical richness–X-ray luminosity distribution function. The vertical planes illustrate its two projections: the cluster richness distribution function and the X-ray luminosity function. All variables are shown in logarithmic representation. A sample of clusters selected by their X-ray luminosity would be drawn from a neat wedge of the luminosity function. However, our sample of clusters is selected according to an optical richness criterion. This is illustrated by the dashed line in the horizontal plane. The resulting deformation to the luminosity function is shown: the sharp cut-off is now smoothed out.

statistical uncertainties in determining the Bahcall richness, this figure must represent an upper limit to the true scatter. Indeed, the original data of Bahcall (1977) suggest a flattening of the correlation for luminosities below $\sim 10^{44}$ erg s^{-1}, and a corresponding increase in scatter, but this effect may simply reflect the statistical uncertainty when the number of galaxies counted becomes very small.

As we shall see, the scatter in the correlation between X-ray luminosity and optical visibility is the dominant source of uncertainty in this work. In order to form a working hypothesis, we shall assume a factor of 2–3 scatter (rms) in L_X for clusters with the same CEMM overdensity, and proceed by parametrizing our results in terms of this quantity. For a scatter of a factor of 3, the $\pm 1\sigma$ quantiles are separated by almost an order of magnitude in luminosity. Although we appear to assume that the slope of the local correlation between richness and X-ray luminosity can be applied at $z \sim 0.5$, in fact the method used is only sensitive to the scatter (in luminosity at a given richness) about this relation.

3 MAXIMUM-LIKELIHOOD METHOD

As we describe below, the *ROSAT* X-ray data have been processed to determine photon count-rates in pre-determined areas centred on the optical position of each cluster. Because the positions are known independently of the X-ray information, detections are not essential in order to extract useful information. By comparing the on-source count-rate in the region of the optical position with that in the surrounding area, constraints on the high-redshift cluster XLF can be derived using a likelihood ratio test (e.g. Cash 1979).

The process begins with an assumed (trial) luminosity function. Allowing for the cluster redshift, Galactic absorption and the fraction of the cluster flux falling outside the detect-cell, the probability distribution of the mean (expectation) on-source count-rate is determined. In order to analyse the measured rate, the probability distribution of the expectation count-rate is convolved with the appropriate Poisson distribution (allowing for the measured background count-rate). By using the *total* count-rate, we avoid having to distinguish between cluster and background photons. The computed likelihood thus allows for the possibility that a high count-rate may arise from a low-luminosity cluster where a statistical fluctuation has resulted in an unusually high number of background photons. Our method is preferable to the survival statistic approach (e.g. Avni et al. 1980), because it does not introduce an artificial distinction between detections and upper limits (cf. Marshall 1992). The calculation is made for each cluster, and the results are combined to give an overall likelihood. Alternative luminosity functions can be assumed, and the relative likelihoods provide a statistical measure of their *relative* compatibility with the data.

In practice, we are most interested in comparing the data with the present-day XLF in order to assess earlier claims for evolution. Using a conventional definition of likelihood, $S = -2 \ln P$, the likelihood-ratio statistic, $S - \min(S)$, is (approximately) distributed as χ^2_ν where ν is the number of free parameters contained in the model luminosity function. Here we adjust only the *amplitude* of the luminosity function, keeping its *shape* fixed with the present-day form. The 95.4 per cent (2σ) and 99.9 per cent (3σ) confidence intervals for the amplitude are defined by the regions in which $S - \min(S) \leq 4.0$ and 9.0, respectively.

As discussed in Section 2, if we account for the locally observed scatter in the L_X–optical richness relation, we can explore the consequences of assuming that our richness-limited sample approximates to an X-ray-flux-limited one. We model this effect by convolving [in $\log_e$(luminosity)] the XLF with a Gaussian of rms width σ (where $\sigma = \ln(2)$, $\ln(3)$, etc.). Including the effect of a low-end cut-off in the luminosity function (due to the finite total number of clusters), this leads to a modified *differential* luminosity function of form

$$F(x)\,\mathrm{d}x = A' x^{-\alpha'} \times \left(\frac{1 + \mathrm{erf}[(\ln x - (\alpha' - 1)\sigma^2 - \ln x_0)/\sigma\sqrt{2}]}{2} \right) \mathrm{d}x,$$

where A' and α' are the *differential* luminosity function's amplitude and slope, respectively, and the cut-off parameter, x_0, is chosen so that the integrated number density agrees with that of the CEMM sample. Note that the convolution process increases the amplitude of the *original* luminosity function by a factor $\exp[(\alpha' - 1)^2\sigma^2/2]$, but this has been incorporated into A'. The magnitude of this term is, effectively, a measure of the difference in the X-ray properties of optical and X-ray-selected cluster samples.

4 ANALYSIS

This project is principally based on the analysis of deep, pointed *ROSAT* images, specifically targeting the CEMM distant clusters. At the present time, we have secured deep, pointed exposures with *ROSAT* for 12 of the sample of 14 clusters described in Section 2. We shall supplement these pointed data with exposures for the two remaining clusters taken from the All Sky Survey. To summarize the selection criteria: these clusters have redshifts based on two or more galaxies, and the sample has been restricted to the redshift range 0.3–0.5, where the CEMM clusters have approximately constant, comoving number density.

In pointed mode, the on-axis point spread function of the *ROSAT* X-ray telescope is sharp (24 arcsec FWHM). Thus clusters at redshift 0.4 should be resolved (although the photon-detection statistics make it unreliable to classify clusters in this way). We have therefore used a detect-cell of 3×3 arcmin^2 in order to ensure that a large fraction of the cluster emission is collected. Assuming a core radius of 0.25 Mpc (cf. H92) at $z = 0.4$, this box includes > 70 per cent of the cluster flux (for the range of off-axis angles covered by our clusters). The narrow redshift interval and small derivative of the angular diameter–redshift relation imply only a small error in applying the same correction to all the clusters. In order to be able to apply our maximum-likelihood method directly to the photon counts, we have not attempted to perform any source-fitting, such as that used in the *ROSAT* Standard Analysis Software (e.g. Cruddace, Hasinger & Schmitt 1988). The background photon count-rate has been determined by spline-fitting the large-scale background variations, after masking out the rib structure and point sources detected with the Extended Standard Analysis Software. This background count is not directly subtracted from the on-source photon count, but is instead

included in our maximum-likelihood model. This allows sources where the on-source count-rate lies below the interpolated mean to be dealt with correctly. The region over which the flux is measured is much greater than the likely astrometric uncertainty (6 arcsec rms), although we were able to check the astrometry independently in most cases, using quasars selected from the NASA NED data base. The large size of our detect-cell makes contamination of the predefined region by nearby point sources a possibility. In the case of J1556.15BL, we were forced to subtract the core emission (a 0.5×0.5 arcmin^2 region) from a point source lying on the edge of the cluster detect-cell.

The details of the *ROSAT* All Sky Survey have been discussed by Trümper (1985). The survey is constructed by processing photon detection events and telemetry information obtained from a continuous scan across the sky. As a result, the point spread function (PSF) associated with each photon is sensitive to the angle between the source and the telescope pointing direction. On axis, the PSF is better than 24 arcsec (FWHM), but it degrades to more than 5 arcmin at large off-axis angles (Hasinger 1985). We determined the source count rate for a 4×4 arcmin^2 box centred on the cluster's optical position. Allowing for the mean survey PSF and the intensity profile of the cluster, this region will contain ~50 per cent of the total source counts. Because of the large size of the detect-cell, we have again neglected uncertainties in the telescope pointing. The background count-rate is determined from a surrounding ring of 30 arcmin mean diameter which was manually checked for contamination from bright sources. Because of the low exposure times, faint point sources cannot be resolved out of the background. Experiment with randomly selected areas showed that the background fluctuations are nevertheless well described by Poisson statistics.

The photon-count statistics of the CEMM clusters are summarized in Table 1. Entries in the table include the vignetting-corrected exposure time, the *background-subtracted* photon counts, the spline-fit background counts, the correction factor for flux falling outside the detect-cell, and the X-ray luminosity in the 0.5–2.5 keV band. The conversion from count-rate to luminosity is made assuming a cluster temperature of 5 keV, although all temperatures in the range 2–10 keV give conversion factors that differ by less than 3 per cent. Where the cluster has been detected at

Table 1. X-ray luminosities of Couch et al. distant galaxy clusters.

Cluster	Redshift (1)	N_H (2)	Exposure (3)	Mode (4)	Cts (5)	Backgr (6)	Det.Lim. (7)	f_{det} (8)	C_L (9)	luminosity (10)
J2175.23C	0.40	1.4	19.77	P	20.	53.	(18.2)	0.7	0.108	0.156
J2175.15TR	0.41	1.4	11.50	P	45.	26.	(12.7)	0.7	0.116	0.648
J1556.15BL	0.457	1.2	29.91	P	45.	748.	(68.4)	0.7	0.145	(0.473)
J2001.21C	0.413	2.9	21.65	P	1. †	43.	(16.4)	0.7	0.132†	(0.142)
J1834.8BL	0.445	3.5	13.15	P	47. †	30.	(13.7)	0.7	0.158†	0.807
J1836.3CR	0.416	2.3	14.75	P	32.	38.	(15.2)	0.7	0.123	0.381
F1652.20CR	0.41	3.2	15.10	P	34.	66.	(20.2)	0.7	0.123	0.396
F1652.22CR	0.48	3.2	15.07	P	18.	64.	(20.0)	0.7	0.172	(0.326)
F1835.2CL	0.377	3.9	17.20	P	−8. †	37.	(15.2)	0.7	0.112†	(0.141)
F1835.22CR	0.469	3.9	21.30	P	19. †	42.	(16.2)	0.7	0.179†	0.228
F1835.28BR	0.346	3.9	14.70	P	13. †	29.	(13.5)	0.7	0.093†	(0.122)
F1637.23TL	0.48	1.1	23.98	P	48. †	39.	(15.6)	0.7	0.174†	0.496
J2172.17C	0.348	1.9	0.347	S	2.4	2.6	(4.4)	0.5	0.083	(2.10)
J2090.7CL	0.38	3.6	0.449	S	−0.3	2.3	(3.7)	0.5	0.105	(1.73)

Note.

(1) In order to be included in the sample, the cluster redshift must be based on at least two cluster members.

(2) Hydrogen column density towards cluster (from Stark et al. 1992), in units of 10^{20} atom cm^{-2}.

(3) Exposure time in ks, corrected for telescope vignetting.

(4) P = pointed-mode observation; S = All Sky Survey observation.

(5) Photon count in detect-cell after background-subtraction. Where marked †, the photon count is measured in channels 52–201, otherwise in channels 41–240. For pointed data, a detect-cell size of 3×3 arcmin^2 has been used; All Sky Survey data use a larger detect-cell (4×4 arcmin^2), to allow for the wider point spread function.

(6) Background count determined from spline fit (pointed observations) or mean of surrounding area (All Sky Survey observations).

(7) Photon count (in excess of background) required for 99 per cent confidence detection.

(8) Fraction of cluster flux assumed to fall within the detect-cell.

(9) Conversion factor from count-rate (in units of 10^{-3} photon s^{-1}) to rest-frame luminosity in 0.5–2.5 keV band (unit = 10^{44} erg s^{-1}). Conversion to flux in the observed 0.5–2.5 keV band may be made by multiplying the count-rate by a factor of 1.5×10^{-11} erg cm^{-2} (channels 52–201) or 1.4×10^{-11} erg cm^{-2} (channels 41–240).

(10) Cluster luminosity in the 0.5–2.5 keV band (in the cluster rest-frame) in units of 10^{44} erg s^{-1}. Where the cluster is detected with better than 99 per cent confidence, the luminosity is calculated as [background-subtracted count-rate] $\times C_L/f_{det}$. Where the cluster is not detected, the flux corresponding to the 99 per cent detection threshold is given.

better than 99 per cent confidence, we have tabulated the inferred luminosity; where no detection has been made, the detection limit is given in brackets. It must, however, be emphasized that the luminosities and detection limits given here are for illustrative purposes only; the maximum-likelihood technique we have described in Section 3 is applied to the photon statistics directly.

Seven of the 12 clusters are detected with more than 99 per cent confidence, but the fluxes are consistently low. All but two of the clusters observed in the pointed mode have luminosities below 5×10^{43} erg s^{-1}, and neither of the remaining clusters is even marginally detected in the All Sky Survey. Given that the effective volume probed by this subset of the CEMM clusters is 2.1×10^{7} Mpc^{-3}, we can calculate the expected luminosities of our clusters from number density considerations [i.e. by inverting the relations $V\,n(>L_1)\approx N$ and $V\,n(>L_2)\approx 1$ for the luminosities L_1 and L_2, where N is the number of clusters in the volume-complete sample, V is volume of the survey, and $n(>L)$ is the cumulative luminosity function]. Thus, if we expected the clusters identified by CEMM to be the brightest X-ray clusters in these areas, we would expect their luminosities to be in the range $5\times10^{43}-5\times10^{44}$ erg s^{-1}. Our data immediately show that these clusters are underluminous by comparison with their present-day counterparts.

The likelihood technique described in Section 3 allows us to provide a quantitative restraint on the XLF amplitude at $z\simeq0.4$. Assuming a *cumulative* XLF in the 0.5–2.5 keV band of the form

$$n(>L)=A\left(\frac{L}{10^{44}\ \mathrm{erg\ s^{-1}}}\right)^{-\alpha},$$

with $\alpha=1.19$ as for the EMSS (H92), we obtain the likelihood curves plotted in Fig. 3. These curves show the significance with which various XLF amplitudes can be ruled out. The different line styles show the effects of various assumptions concerning the tightness of the correlation between X-ray luminosity and optical richness.

In the case of a tight correlation between X-ray luminosity and optical richness, the positive detections define a best-fitting solution whose amplitude lies approximately a factor of 10 below the low-redshift equivalent measured by H92 ($A_{\mathrm{H92}}=3.13\times10^{-7}$ Mpc^{-3}). The introduction of scatter into the L_X-richness relation (see Section 3) weakens the result. Nevertheless, for a factor of 2 scatter at fixed richness, as suggested by the observations of Edge & Stewart (1991a), the formal uncertainty in the solution is still small: $A=0.6\pm0.3\times10^{-7}$ Mpc^{-3} (1σ error). The no-evolution amplitude is excluded with $>5\sigma$ confidence.

However, the precision of the test is naturally undermined if a larger scatter parameter is considered. If the scatter is increased to a factor of 3, two effects become notable. First, there is an increased chance that the low luminosities of the pointed-mode observations are not representative of the mean L_X–optical richness correlation. Secondly, there is an

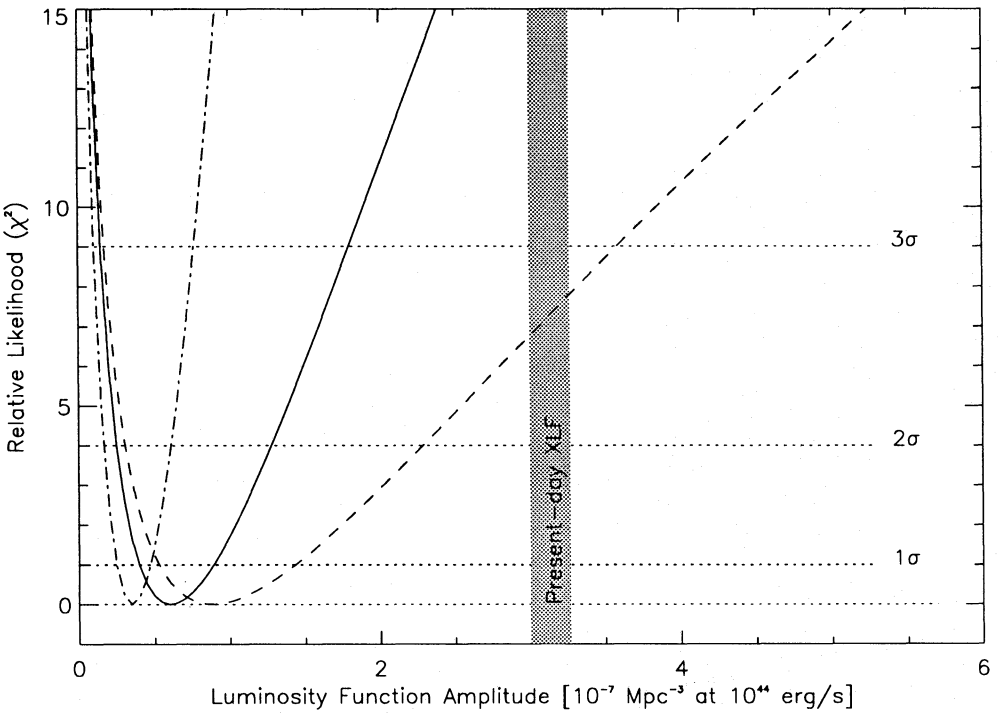

Figure 3. Likelihood curves for the combined data set consisting of 12 clusters observed with deep, pointed *ROSAT* exposures, plus two further clusters examined using the All Sky Survey. The curves plot the relative likelihoods of different amplitudes of the luminosity function (as defined in Section 3). The luminosity function slope, α, is fixed at 1.19. The varying line styles distinguish different assumptions about the correlation between optical richness and X-ray luminosity: dot-dashed line: perfect correlation; solid line: factor of 2 scatter in X-ray luminosity at a given richness; dashed line: factor of 3 scatter. Data on nearby clusters suggest that a factor of 2 scatter in X-ray luminosity may be most appropriate.

offset between the median luminosity of clusters of given richness and the X-ray luminosity of clusters at the equivalent number density. Basically, this effect arises because a Gaussian convolution of the XLF alters its amplitude (Section 3) in a manner similar to the Malmquist bias familiar in optical astronomy. In this case, the data are inconsistent with the no-evolution model at about the 99 per cent confidence level.

5 DISCUSSION

The cumulative XLFs plotted in Fig. 4 summarize our main result. The low-redshift XLF derived by H92 from the EMSS has been converted to cumulative form and transformed to the 0.5–2.5 keV band, assuming a mean cluster temperature of 5 keV. For reference, we also show the data points derived from our individual pointed exposures. These have been plotted as number densities by calculating the fraction of the total volume associated with an individual cluster, and ordering the clusters (in cumulative density space) by their measured luminosity (the approach parallels the calculation used to estimate the expected range of cluster luminosities in Section 4). Where a cluster has not been detected, we have plotted the 99 per cent detection limit (arrowed points). While it is a convenient way to represent our data, this technique does not enable us to estimate the uncertainties easily. To do this, we use the maximum-likelihood analysis described earlier; thus we have superimposed the 3σ upper limit to the luminosity function derived from the combined All Sky Survey plus pointed data set (adopting a factor of 2 scatter in the L_X-richness correlation, and an XLF slope $\alpha = 1.19$). The discrepancy with the local XLF is emphasized by the shading.

Two previous studies (based on X-ray-selected samples of clusters) have reported evidence for negative evolution of the XLF. Edge et al. (1990) probed a much larger volume of sky in a shallower, flux-limited sample. The evolution they claim is restricted to clusters with luminosities greater than $\sim 6 \times 10^{44}$ erg s^{-1}, which is outside the range of luminosities and volume densities probed by this study. The analysis of the EMSS by H92 is more comparable with this work. We have added their high-redshift luminosity function (median redshift = 0.33) to Fig. 4 as a dashed line. We assume that the difference in redshift between this sample and our optically selected sample is sufficiently small (0.42 versus 0.33) that (as a first approximation) the two luminosity functions may be directly compared. It can be seen that there is good agreement between the two studies: the lower luminosities probed by the EMSS merge smoothly into values of XLF amplitude allowed by our data.

However, the figure suggests that the steeper slope of the $z = 0.33$ H92 XLF cannot be sustained faintward of 10^{44} erg s^{-1}. In view of the complexity of our selection criteria, such conclusions must be examined carefully, using the likelihood statistics developed earlier. The steeper slope of the H92 XLF implies a greater sensitivity to the effects of scatter, as illustrated in Fig. 5; here, instead of comparing our data with the *local* XLF, we make a direct comparison with the $z = 0.33$ XLF of H92.

For a factor 2 scatter, a lower amplitude than that derived by H92 is preferred, suggesting either a break in the XLF slope at around 10^{44} erg s^{-1}, or a strong evolutionary effect

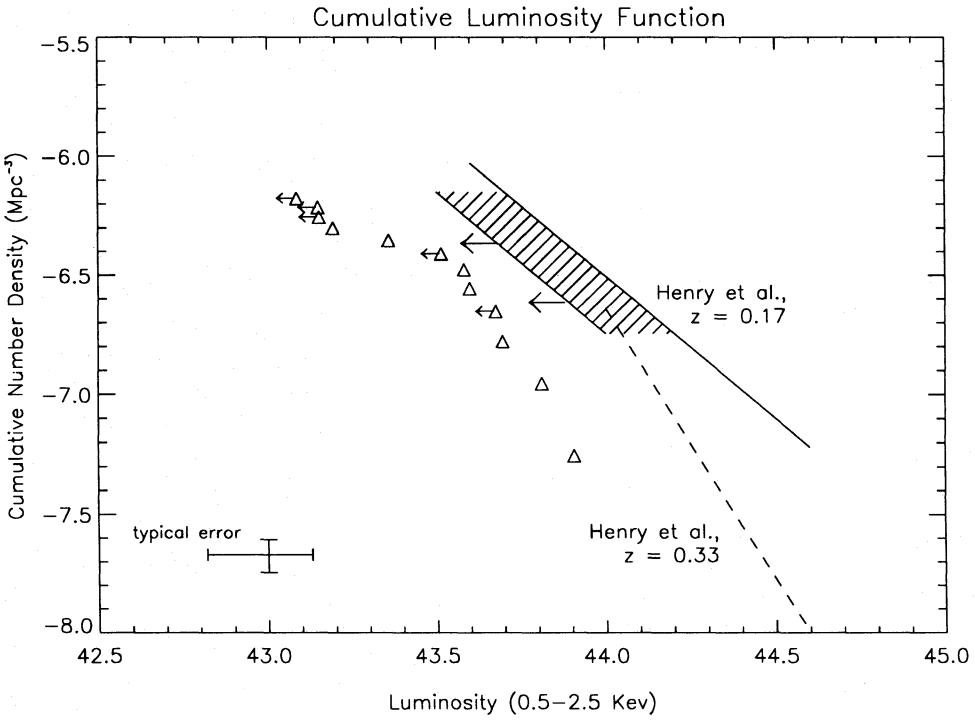

Figure 4. The XLF at various redshifts with derived limits at high redshift from the pointed data discussed in Section 5 (see text for further details).

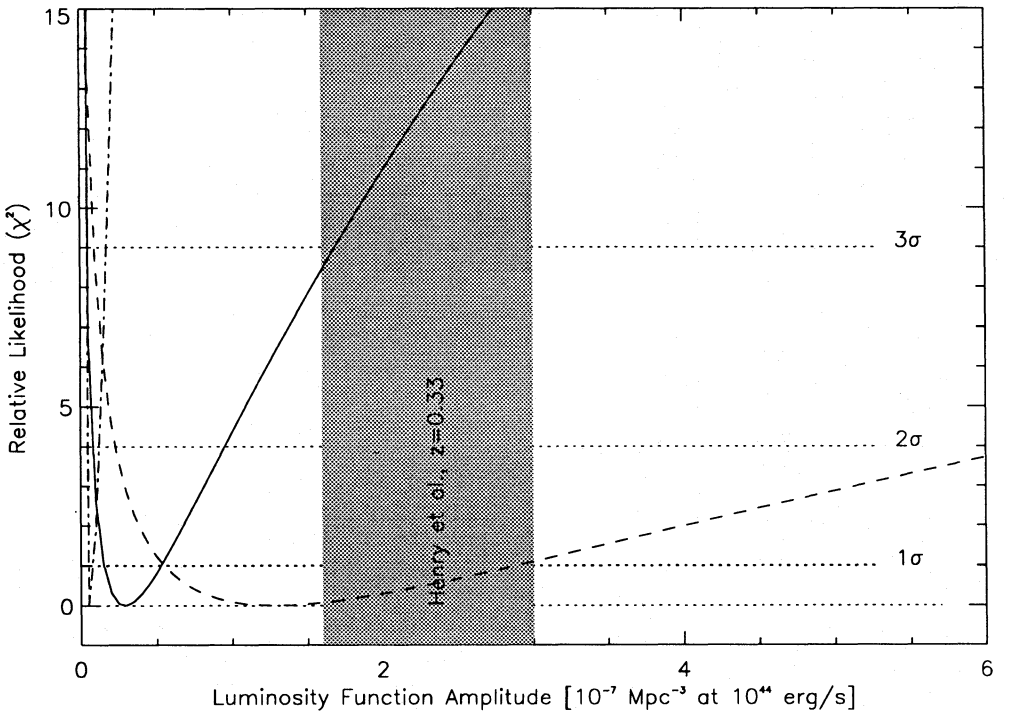

Figure 5. Likelihood curves for the combined data set tested against a steeper luminosity function ($\alpha = 2.27$). The shaded area indicates the range of amplitudes fitting the EMSS sample of high-redshift clusters (median redshift 0.33).

between $z = 0.33$ and 0.42. For a factor 3 scatter, however, almost no constraint at all can be derived, and the optical selection fails, with the current sample, to provide convincing constraints. For steep XLFs with such high scatter, the optically selected and X-ray-selected samples have few clusters in common. Thus, in this case, although continuity with H92's data appears reasonably secure, the precise form of the high-z luminosity function cannot be ascertained with confidence.

6 CONCLUSIONS

We have used *ROSAT* All Sky Survey and deeper pointed observations to investigate the X-ray luminosities of distant galaxy clusters selected from the statistically complete, richness-limited sample constructed by CEMM. The mean redshift of the sample is close to $z = 0.4$, allowing us to test directly earlier claims for evolution in the X-ray luminosity function.

We detect no strong X-ray emission from any of the clusters. If the X-ray luminosity is closely correlated with optical richness, then we determine an amplitude for the $\bar{z} = 0.4$ luminosity function that lies an order of magnitude below the present-day normalization. However, it is important to allow for the scatter in the correlation between optical richness and X-ray luminosity, and so we parametrize our results in terms of this quantity. Local data suggest a factor of 2–3 scatter in L_X at a fixed richness.

We developed a technique to incorporate this scatter into a maximum-likelihood analysis of the bivariate luminosity function. We find that the weak luminosities cannot be consistent with a non-evolving luminosity function, unless the scatter in the L_X–richness correlation is very large. We therefore conclude that there is a significant reduction in the space-density of X-ray-luminous clusters at $z = 0.4$. This is in qualitative agreement with earlier work based on the EMSS.

We compare our results quantitatively with those of the EMSS. As our data probe clusters with volume densities around 3×10^{-7} Mpc^{-3}, they are more numerous than those studied in the EMSS analyses. This means we can investigate possible evolution in the *form* of the luminosity function. Such changes might be expected where the gas content of clusters scales self-similarly with the dark matter distribution (cf. Kaiser 1991).

The EMSS analysis suggests a steeper slope for the luminous end of the XLF at redshifts $z \simeq 0.3$. Extrapolation of this form to lower luminosities is *not* consistent with our data. If correct, this would imply a definite change in the form of the XLF, since $z \simeq 0.3$–0.4. Unfortunately, by virtue of our optical selection, this is not yet a strong result. If confirmed by further analysis of the deep exposures, we may then succeed in ruling out the simplest class of models in which the gas evolves self-similarly with the matter distribution. This would champion models in which the evolution of the XLF is dominated by the development of the gaseous intracluster medium.

Ultimately, the results we have presented rely on there being a viable correlation between the optical visibility of a galaxy cluster and its X-ray properties. The scatter we have assumed – between a factor of 2 and 3 – hides a wealth of perplexing physics (e.g. Cavaliere, Burg & Giacconi 1991). A better understanding of this problem is clearly needed. If the

optical–X-ray correlation is as tight as we have suggested, then our data provide *compelling* evidence for a systematic fall in the X-ray luminosities of rich galaxy clusters at $z \geq 0.4$. The alternative is to assert that the missing fraction of the luminosity function is made up by optically weak clusters. Using data from the *ROSAT* archive, this question is now open to investigation. The next step in this project will be to return to the deep plates, searching for clusters at known X-ray source positions.

ACKNOWLEDGMENTS

We thank Wolfgang Voges and the *ROSAT* data-processing team for the provision of the data on which this paper is based. We also thank Alastair Edge, Carlos Frenk and Pat Henry for the generous time in discussing this work with us. RGB and RSE acknowledge the support of the Science and Engineering Research Council and the Royal Society. FJC acknowledges the support of the Instituto de Astrofísica de Canarias, and HB the support of the Deutsche Forschungsgemeinschaft (Mo 416/1-6). WJC acknowledges the financial support of the Australian Research Council.

REFERENCES

Abell G. O., 1958, ApJS, 3, 211
Abell G. O., Corwin H. G., Olowin R. P., 1989, ApJS, 70, 1
Avni Y., Soltan A., Tananbaum H., Zamorani G., 1980, ApJ, 238, 800
Bahcall N. A., 1977, ApJ, 217, L77
Briel U. G., Henry J. P., 1993, A&A, 278, 379
Cappi A., Chincarini G., Conconi P., Vettolani G., 1989, A&A, 223, 1
Cash W., 1979, ApJ, 228, 939
Cavaliere A., Burg R., Giacconi R., 1991, ApJ, 366, L61
Couch W. J., Ellis R. S., Malin D. F., MacLaren I., 1991, MNRAS, 249, 606 (CEMM)
Cruddace R. G., Hasinger G. R., Schmitt J. H., 1988, in Murtagh F., Heck A., eds, Astronomy from Large Databases. European Southern Observatory, Munich, p. 177
Davis M., Efstathiou G., Frenk C. S., White S. D. M., 1985, ApJ, 292, 371
Edge A. C., Stewart G. C., 1991a, MNRAS, 252, 414
Edge A. C., Stewart G. C., 1991b, MNRAS, 252, 428
Edge A. C., Stewart G. C., Fabian A. C., Arnaud K. A., 1990, MNRAS, 245, 599
Frenk C. S., White S. D. M., Efstathiou G. P., Davis M., 1990, ApJ, 351, 10
Gioia I. M., Henry J. P., Maccacaro T., Morris S. L., Stocke J. T., Wolter A., 1990, ApJ, 356, L35
Gunn J. E., Hoessel J., Oke J. B., 1986, ApJ, 306, 30
Hasinger G., 1985, Bull. Inf. Cent. Données Stellaires, 28, 87
Henry J. P., Gioia I. M., Maccacaro T., Morris S. L., Stocke J. T., Wolter A., 1992, ApJ, 386, 408 (H92)
Kaiser N., 1986, MNRAS, 222, 323
Kaiser N., 1991, ApJ, 383, 104
Lumsden S. L., Nichol R. C., Collins C. A., Guzzo L., 1992, MNRAS, 258, 1
Marshall H. L., 1992, in Feigelson E., Babu G. J., eds, Statistical Challenges in Modern Astronomy. Springer-Verlag, New York, p. 247
Stark A. A., Gammie C. F., Wilson R. W., Bally J., Linke R. A., 1992, ApJS, 79, 77
Stocke J. T., Morris S. L., Gioia I. M., Maccacaro T., Schild R., Wolter A., Fleming T. A., Henry J. P., 1991, ApJS, 76, 813
Trümper J., 1985, Bull. Inf. Cent. Données Stellaires, 28, 81